# Interferometry based technique for intensity profile measurements of far IR beams

Alexander A. Soloviev,* Efim A. Khazanov, Ilya E. Kozhevatov, and Oleg V. Palashov

The Institute of Applied Physics of the Russian Academy of Sciences, 603950, 46 Ul'yanov Street, Nizhny Novgorod, Russia

*Corresponding author: so_lo@appl.sci-nnov.ru

Received 1 November 2006; revised 1 February 2007; accepted 3 February 2007; posted 21 February 2007 (Doc. ID 76595); published 31 May 2007

We present a novel, to the best of our knowledge, method for measuring the intensity profile of far-IR beams. The method is based on the measurements of nonstationary variation in optical thickness of a fused-silica plate heated by the studied radiation. The optical thickness is observed by means of a reflecting interferometer. Purpose-made experimental setup allows one to measure beams with an aperture of up to 60 mm with a spatial resolution of 1 mm. The accessibility of the utilized technologies and the possibility to easily increase the aperture are the major advantages of this approach. The probable area of application for the method is measurements of beams produced by powerful industrial far-IR lasers. 

*OCIS codes:* 040.3060, 140.6810, 120.3180.

## 1. Introduction

A wide variety of methods are currently available for measuring the intensity profile of electromagnetic radiation in different regions of the frequency spectrum. The most developed technology covers devices operating in the visible region based on the photoeffect-photon detectors. Meanwhile, operation of the photon detectors in the mid- and far IR is complicated by the presence of thermal electron emission, and thus, the use of devices exploiting other physical principles is a better choice. In the majority of cases, however, a sophisticated and expensive technology is required to produce such devices.

An IR sensor is basically a rectangular array of independent sensing elements. Such detector arrays are called focal plane arrays (FPAs) [1]. There are photon and microbolometric detector arrays. Photon sensors in the far-IR band require cooling; the longer the wavelength of radiation being studied, the greater the cooling must be. The necessity to employ complex cooling systems cannot but adversely affect consumer-related properties and the cost of the photon sensors. Nonphoton type detectors mainly measure temperature changes of a radiation-absorbing target. Such detectors are usually called microbolometers. The target temperature can be measured using different physical principles. The most common are detectors that are based on the bolometric effect [2] (temperature dependence of conductivity of a material). Also in use are pyroelectric [3], thermocouple, and microelectromechanical (MEMS) [4] detectors. An example of the pyroelectric detector is the II-VI-$CO_2$ Beam Profiler from Spiricon Inc., intended for intensity profile measurements in commercial $CO_2$ lasers.

A number of methods are based on the scanning of the object being investigated with diaphragms of various forms. In this case, it is possible to use, for instance, a line of elements [5] or even a single sensing element rather than an array of detectors. A good example here is the BEAMSCAN device [6] produced by Photon Inc., in which a beam of interest is scanned over two slit apertures.

All of these methods share a common disadvantage of complicated and hence expensive fabrication technology. At present, detector arrays of more than 20 mm are very rare, so for the measurement of larger-diameter beams one needs to use expensive IR objectives. In this paper, we report on an original, to the best of our knowledge, method for measuring in-

0003-6935/07/183821-08$15.00/0

tensity profiles of $CO_2$-laser radiation, which is free from the above disadvantages. The sensing element here is an absorbing plane-parallel plate in which thermally induced variations in optical thickness are measured interferometrically. The interferometer operates in the visible light, so no expensive FPAs are needed for corresponding wavelengths. Moreover, the aperture size is limited only by visible-range optics, which is more widely available than IR optics.

In Section 2, the major foundations of the method are described using the assembled optical setup as an example. In Section 3, the experimental data are presented. In Section 4, the factors limiting the accuracy and the dynamic range of measurements are covered. In Section 5, the achieved characteristics of the method with possible ways of improvement are considered.

## 2. Description of the Method

The method we suggest here is a typical bolometric method. The idea is as follows. Radiation whose intensity profile we intend to measure is directed to an absorbing fused-silica plate, heating it. The temperature nonuniformity leads to variations in optical thickness, which we measure by means of a precision reflectance interferometer [7] in a short period of time after the heating activation. The period should be short enough so that the temperature profile does not have time to blur due to thermal conductivity.

The reason why we have chosen fused silica as the sensing element is that it possesses an advantageous combination of thermo-optical, elastic, and photoelestic constants, which we will discuss in detail in Section 4. In addition, fused silica absorbs well in the range from mid-IR to microwave wavelengths [8]. This feature, in particular, allows for intensity profile measurements of $CO_2$-laser irradiation.

We will discuss in more detail the principle of the profile measurement method, as exemplified in a specially designed optical setup shown in Fig. 1.

The setup can be divided into two parts by its functional features: the part that forms the radiation supposed to be measured (elements from 1 to 7, Fig. 1) and the measuring part (8 to 17 elements).

The radiation is formed in the following way. Radiation from a $CO_2$ laser 1 is attenuated by a disk chopper 2 and is then split into two portions by a saline wedge 3. The weaker, reflected portion is directed to a power meter 4. Due to this, one can continuously control the power of radiation passed through the wedge. Then the radiation arrives at a flat metallic mirror 5 and a spherical metallic mirror 6. The shutter 7 ensures maximally fast heat activation. Because of the effect of thermal conductivity, the temperature profile blurs over time relative to the heating radiation profile, thereby worsening the spatial resolution of the method. The spatial resolution can be improved by reducing the time after heat activation (the shutter opening). By moving the spherical mirror 6, we varied the transverse size of heating radiation incident on the surface of the fused-silica plate 8. Note that the laser radiation at 10.6 μm is absorbed by fused silica in a thin subsurface region with a typical depth of ~30 μm that practically corresponds to the surface heating.

This scheme allows one to provide a power range from units of milliwatts to 20 W and practically an arbitrary beam size on the aperture of the fused-silica plate 8. It corresponds to an intensity range that undoubtedly exceeds the dynamic range of the method. With increasing output power of a $CO_2$ laser, the spatial intensity distribution becomes broader and more complex, since the laser now operates in the multimode regime (not an adverse factor in our situation).

The variations in optical thickness of the fused-silica plate were measured by a reflectance interferometer. It is better to discuss its design in more detail. Radiation from a probe helium–neon laser 9 after collimating objective 10 comes to the fused-silica plate 8 and reflects from its front and back faces. The reflected beams are spatially matched in a wavefront conjugation unit 11 that consists of two semitransparent mirrors 12 and 13. Unwanted reflections from the conjugation unit 11 are filtered out by an angular

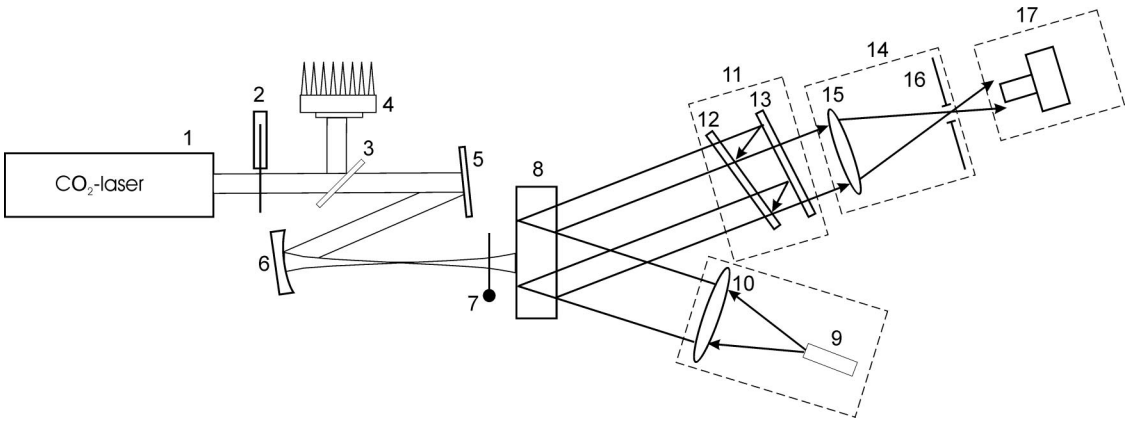


Fig. 1. Optical setup layout: 1, $CO_2$-laser; 2, disk chopper; 3, saline wedge; 4, bolometric power meter; 5, flat metallic mirror; 6, spherical metallic mirror; 7, mechanical shutter; 8, fused-silica plate; 9, helium–neon laser; 10, objective; 11, wavefront conjugation unit comprising semi-transparent mirrors 12 and 13; 14, angular filter comprising objective 15 and pinhole 16; 17, CCD camera.

filter 14 consisting of an objective 15 and an aperture 16. The interference pattern is recorded by a CCD camera 17 with a 25 frame per second frequency and analyzed by a computer.

This interferometer makes phase-modulated measurements of the optical thickness of a sample with record-breaking accuracy ($\sim\lambda/1000$) [9]. To achieve this, the path-length difference between interfering rays is mechanically varied using displacement of the mirror 12 in the conjugation unit 11 (see Fig. 1). The computing algorithm uses not less than 12 consecutive frames to find the optical thickness profile. The assumption that the changes in optical thickness during the measurement are small is also utilized. Such computing permits us to determine the modulation depth, thereby considerably improving measurement accuracy, and removing the uncertainty related to the nonmonotonic dependence of the interference pattern with respect to the phase difference.

Unfortunately, the measurement of unstable variation in optical thickness is connected with the following circumstances (these circumstances are not related to the phase-modulated measurements, in general, but rather to their particular realization in our experiments). First, significant errors occur when the changes in optical thickness during the measurement time are comparable with the wavelength of the probe radiation. Second, utilizing a big number of frames increases the time period from the heating activation and thereby degrades the spatial resolution.

In this connection, the measurements were carried out in two stages. At the first stage, the modulation depth of the interference pattern was determined by means of phase-modulated measurements. After that, mechanical modulation of the path-length difference of interfering rays was switched off and heating was activated. At the second stage, heat-induced variations in the optical thickness were measured using a simple one-frame interference technique (without modulation of the phase), taking into account information on the modulation depth that improves accuracy. Conversion to this combination of interferometric measurements allowed us to reduce the measurement time from 480 to 80 ms (from 12 frames to 2 frames).

### 3. Experimental Results

In this section, we present the results of several series of experiments that permit us to estimate the dynamical range and spatial resolution of our experimental setup.

In the first experimental series, we measured variations in the optical thickness $\Delta L(x, y)$ induced by heating beams with power $P$ ranging from 0.33 to 14 W for the time after heating is activated $t_m$ = 80 ms. Typical beam sizes depended on laser power in the range of 1.5–4 mm. Figure 2 shows variations in

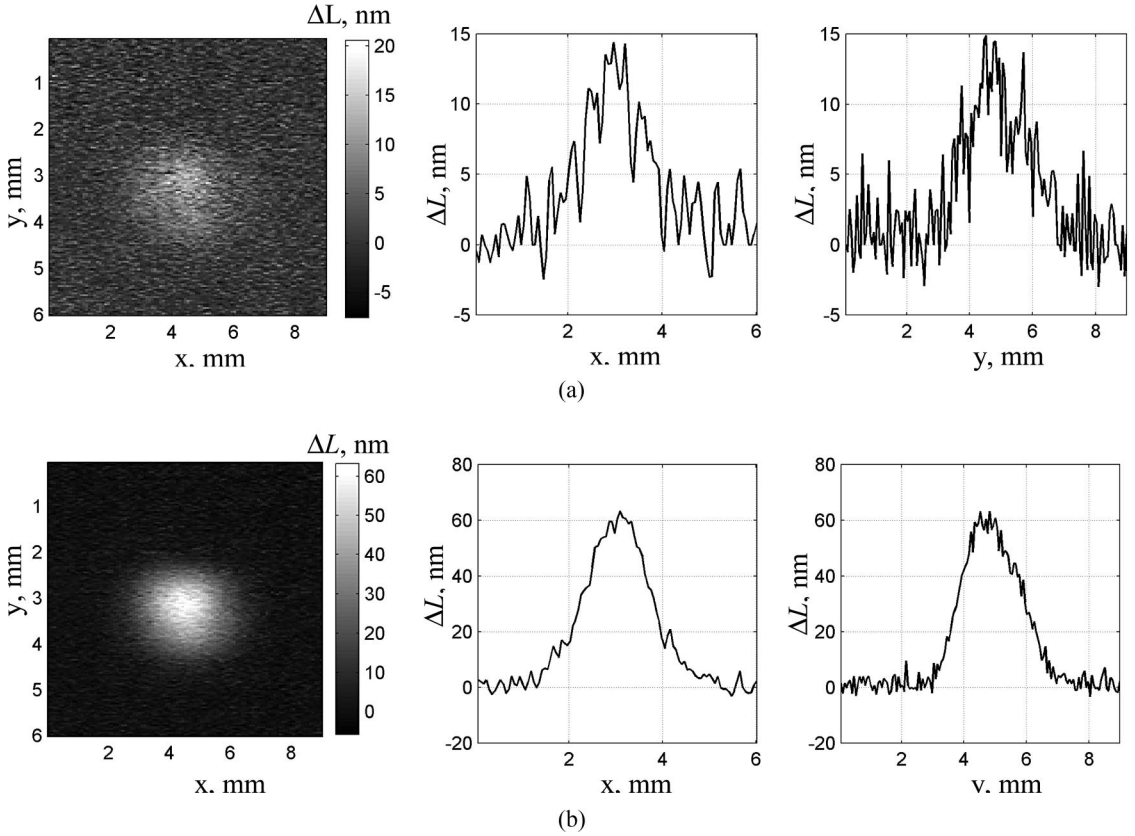


Fig. 2. Optical thickness variations corresponding to intensity profiles of beams with power 330 mW (a) and 1.8 W (b). Topograms (left pictures) and their horizontal (middle pictures) and vertical (right pictures) cross sections are presented.

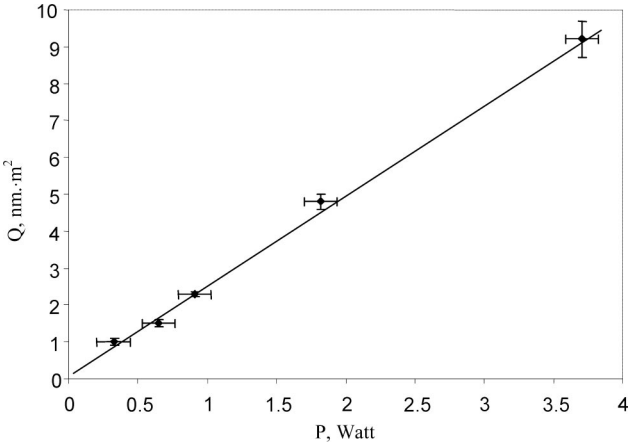


Fig. 3. Experimental test of linearity. Heating beam power is plotted on the horizontal axis, and overall heat-induced variations of the optical thickness on the vertical axis.

optical thickness corresponding to beam intensity profiles for two values of the laser power ($P$ = 0.33 W and $P$ = 1.8 W). Optical thickness variations not exceeding a quarter of a wavelength correspond to laser powers up to 3.8 W.

Data used for plots in Fig. 2 were also used to test the linearity of the method. Figure 3 is a plot showing power directly measured by power meter 3 (see Fig. 1) along the $x$ axis and overall variations of the optical thickness $Q$ along the $y$ axis.

$$Q = \int \Delta L(x, y)\mathrm{d}x\mathrm{d}y, \tag{1}$$

where integration is performed over the whole aperture of the interferometer. The figure shows that the method is well linear in the interval from 330 mW to 3.8 W of total power. The lower bound is due to noise in the camera and in the frame grabber. The upper bound is determined by the violation of monotonic dependence of the interferogram at high intensities (see below). In Fig. 2(a), which we considered as the lower threshold of power sensitivity, the signal-to-noise ratio is ~3. Further, we introduce a coefficient, which is equal to the slope of the obtained line $k = Q/P$ and has the sense of method sensitivity.

The conversion to a combination of phase-modulated and one-frame measurements (see Section 2) allowed us to improve temporal resolution but limited the dynamical range, which is due to the interference pattern, which becomes nonmonotonic at high intensities. As a result, a special procedure was required for adequate processing of optical thickness variations exceeding a quarter of a wavelength of probing radiation. The procedure consisted of dividing the interferogram into monotonic regions, which were joined based on the assumption of relative smoothness of the variation profile and information from subsequent frames. One time the procedure was performed for 14 W of power. The result is shown in Fig. 4.

The plot in Fig. 4 qualitatively correctly shows variations of optical thickness in two monotonic regions, which were joined. But there is a noticeable discontinuity (indicated by ovals in the figure) at the boundary between these regions, which we attribute to poor quality of optics used in the interferometer (see Section 4 for details). Thus, we considered this joining procedure as unsatisfactorily performed, and at that stage of our investigation, we limited ourselves to a power range in which the optical thickness variations did not exceed a quarter of a wavelength of probing radiation (i.e., they occupied one monotonic region).

In the second series of experiments, we studied the spatial resolution of the method limited by temperature profile blurring due to thermal conductivity. In doing this, we measured a beam profile, with part of the beam being shielded by a metal plate very close to the fused-silica surface to avoid diffraction blurring of the intensity jump. From experiment to experiment, the total beam power varied in the range from 300 mW to 14 W. The results of these experiments are presented in Fig. 5. The joining procedure of the monotonic regions was not performed in this series of experiments because it would have no effect on the boundary width.

As can be seen in Fig. 5, the boundary width is ~1 mm. The measurements showed that it does not depend on the amplitude of the intensity jump. It

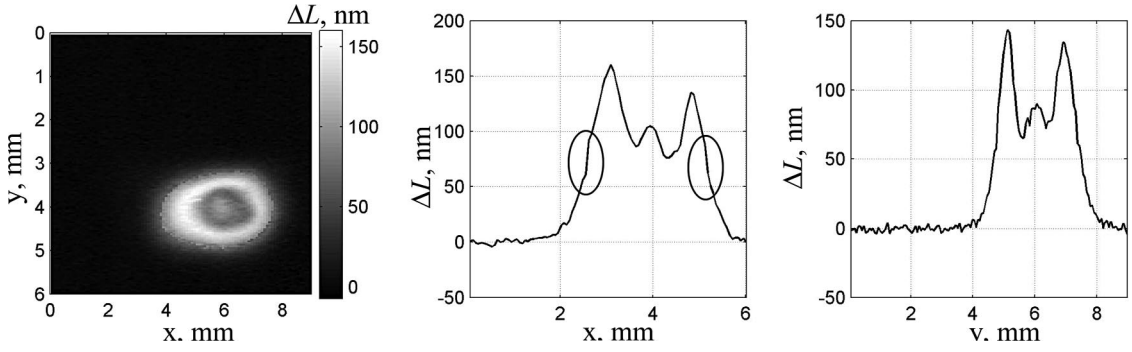


Fig. 4. Plot of optical thickness variations under heating by a $CO_2$ laser beam with power 14 W. Picture on the left is a topogram; the middle and right pictures represent vertical and horizontal cross sections, respectively. The procedure of nonmonotonicity removal was performed once. The ovals show discontinuities due to poor quality of optics.

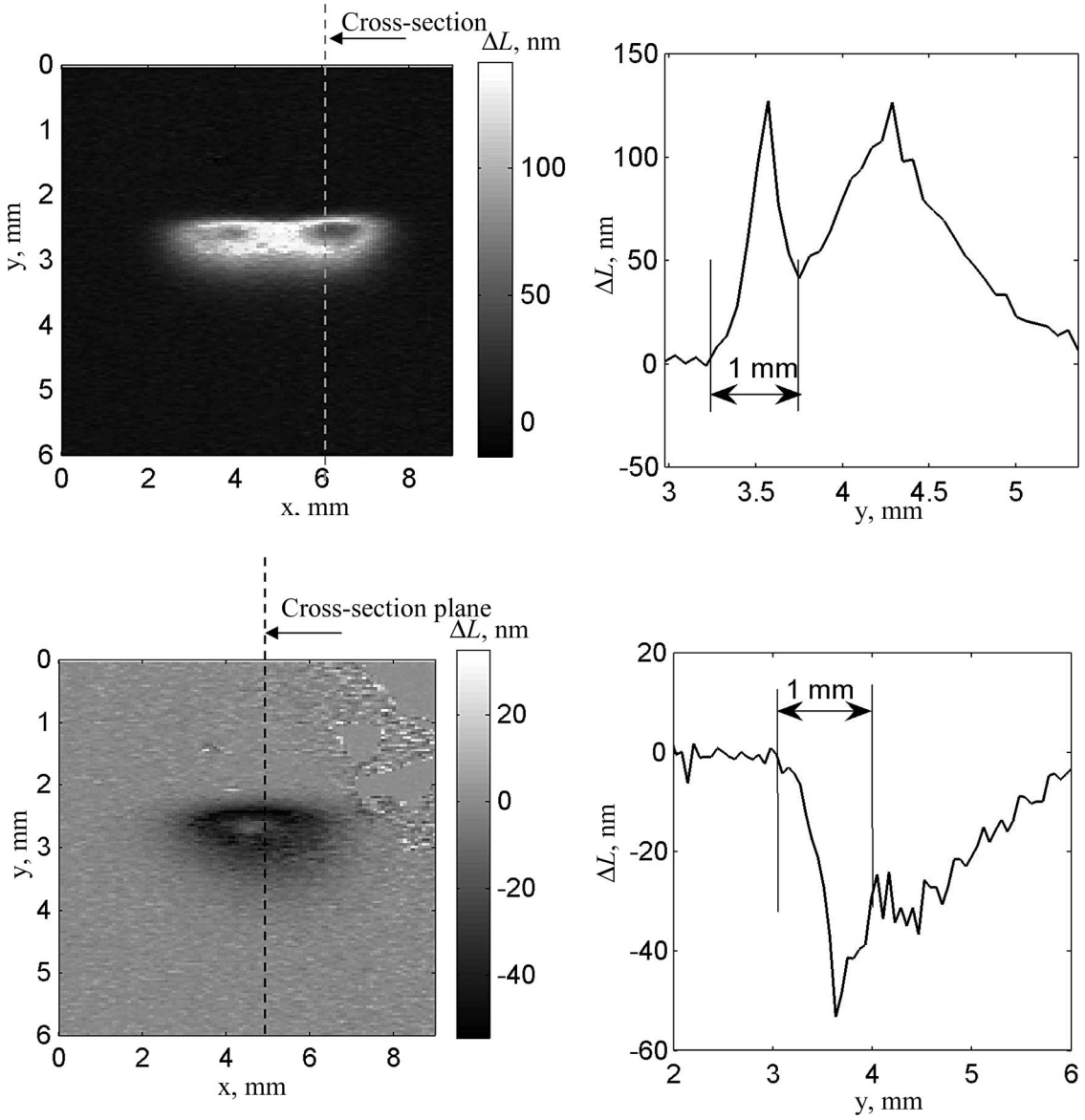


Fig. 5. Variations in optical thickness caused by heating beams with a sharp jump in intensity profile (a topogram on the left and its vertical cross section on the right). Total power of beams: 12.6 W on top, 0.6 W on bottom. The joining procedure is not performed.

could be anticipated that according to the thermal conductivity equation [10], relative blurring of the temperature profile depends only on the time period from heating activation. The experimental value of blurring width agrees well with the calculated one (see Section 4).

It should be noted that an alternative measurement of the $CO_2$-laser irradiation profile was performed by means of a chink diaphragm scanning the beam that is directed at the bolometric power meter. Such a measurement was described by Zelenogorsky [9]. It is significant that this method expects a rather long measuring time (time for shift of the diaphragm plus responding time of the power meter in each point) apart from averaging the profile along the direction of the chink. Nevertheless, the width of a beam measured by the moving diaphragm and the one measured by the described interferometric method were in good agreement.

#### 4. Limiting Factors

The experimental results demonstrate the viability of the method. At the same time, the characteristics we achieved can be considerably improved. For these purposes, one needs to change the existing optical setup, taking into account factors that we will discuss in this section.

The factors limiting the spatial resolution and dynamical range fall into two groups. The factors of the first group are connected with physical processes occurring in the heated fused-silica plate. These are physical factors. One can refer to them as differences between optical thickness variation profiles and intensity profiles of heating radiation, and limitations

associated with possible target overheating. The second group factors are measurement factors related to the accuracy of interferometric measurements. This group includes maximal and minimal intensity limitations associated with measurement accuracy of nonstationary variations of optical thickness.

The impact of the first-type factors was estimated by numerical modeling. We used a specially developed code [9,11] based on solving equations of thermal conductivity [10] and elastic statics of solids [12]. This code finds nonstationary temperature fields and corresponding stresses and deformations in a cylindrical sample heated by cylindrically symmetric sources. The heat sources may be both on the surface and at the bulk of the sample.

### A. Physical Factors

The major factor limiting spatial resolution of the method is the distinction between the profile of optical thickness variations and heat intensity profile. Two reasons for this distinction can be noted. First, the temperature profile blurs due to thermal conductivity. Second, variations in optical thickness are related to both the temperature dependence of refractive index whose contribution replicates the temperature profile and the elastic stress with a more complex contribution. Let us consider these reasons more comprehensively.

At the very beginning of heating, the temperature profile replicates a heat source profile, but the occurrence of noticeable temperature gradients leads to heat removal from more heated sites, eventually blurring the pattern. This circumstance was studied by numerical modeling. We numerically modeled surface heating by a heat source with a sharp jump in its distribution function. Since our program is limited by cylindrical symmetry, we modeled heating in the form of a round spot placed coaxially to the end face of the fused-silica sample. Intensity was constant inside the spot and zero outside. Figure 6 shows the time dependence of the width of optical thickness jump $\Delta x$ for the different radii of the heating spot. The width was measured from the 90% to the 10% level. The plot indicates that to adequately observe a radiation profile with the size of inhomogeneity not less than 1 mm, one needs to make measurements no longer than 120 ms after heating activation. It is also seen that the speed of blurring at the times we are interested in weakly depends on the radius of the heating spot. The estimates verified by experimental data (see Section 3) become the reason why we abandoned the basic phase-modulated measurement scheme in favor of the faster, though less accurate, combination of phase-modulated and one-frame scheme. It allows us to reduce the heating time from 480 ms (12 frames) to 80 ms (2 frames).

Let us consider the contribution made by elastic-stress-related effects to the optical thickness variations. The variations of optical thickness in fused silica are described by the expression [13,14]

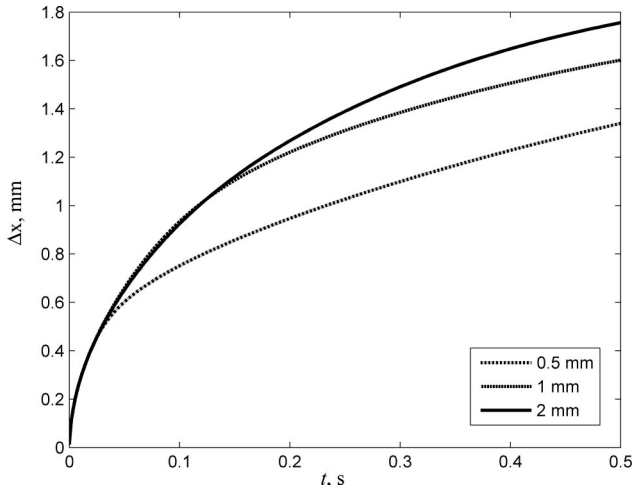


Fig. 6. Dependence of the jump width of optical thickness on time of heating. Intensity profile of heating radiation has a sharp jump. Dash-dotted curve corresponds to 0.5 mm radius of the heating spot, dashed curve corresponding to 1 mm radius, solid curve corresponds to 2 mm radius.

$$\Delta L(x, y)_i = \int_0^l \left\{ \beta T(x, y, z) + n_0 \varepsilon_{zz} - \frac{1}{2} n_0{}^3 \pi_{iikl} \sigma_{kl} \right\} \mathrm{d}z, \tag{2}$$

where integration is performed over a probe beam trajectory coinciding with the $z$ axis, $n_0$ is the refractive index at ambient temperature, $T(x, y, z)$ is the temperature difference to the ambient temperature, $\beta - \mathrm{d}n/\mathrm{d}T$, $\varepsilon_{ij}$ is the strain tensor, $\sigma_{ij}$ is the elastic stress tensor, $l$ is the length of a sample, and $\pi_{ijkl}$ is the tensor of photoelastic coefficients. Optical thickness depends on polarization of radiation because of thermally induced birefringence. The ordinary and extraordinary waves correspond to index $i$ equal to unity or twain, respectively. The directions of polarizations are bound to the proper frame of reference of the strain tensor $\varepsilon_{ij}$.

The terms in brackets have the following sense: the first term is responsible for the dependence of refractive index on temperature, the second is responsible for geometrical change of the sample thickness, and the third is responsible for the photoelastic effect. The terms were assayed numerically in the case of heating by the source whose intensity distribution has a sharp jump (see above). For fused silica, the contribution of the second and third terms after 120 ms of heating does not exceed 5% of the total sum. It means that the curve on Fig. 6 without the contribution of these terms is slightly different than the plotted one. This fact was utilized in the work [11] for fine adjustment of the experimental setup which compensated aberrations by means of additional heating by $CO_2$ laser radiation. In [9], analogous estimates allowed us to compare data obtained with the scanning Hartmann sensor and those with the optical interferometer. Such a result is valid for arbitrary polarization of through-passing radiation. As a result, the optical

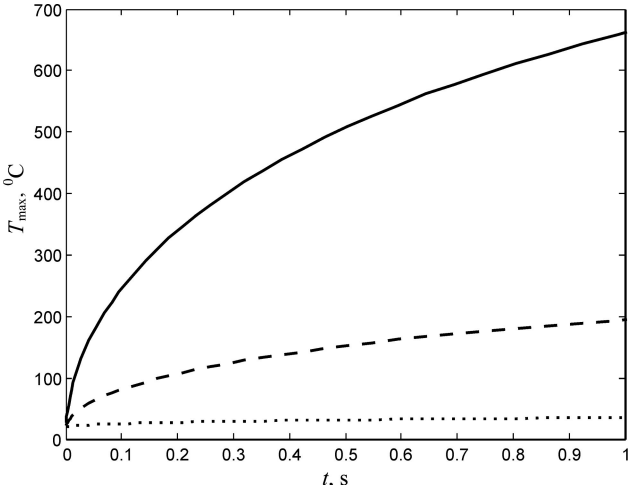


Fig. 7. Dependence of maximum temperature in a sample on time of heating by a Gaussian beam with a radius of 2 mm and powers of 14 W (solid curve), 3.8 W (dashed curve), and 0.33 W (dotted curve).

thickness (measured interferometrically) with high accuracy repeats the temperature profile averaged over the $z$ axis. This temperature profile is close to the heating profile.

In addition, possible overheating of the plate was numerically studied. We plotted (see Fig. 7) dependences of maximum temperature in a sample on time from heat activation when heating by a Gaussian beam with a diameter of 4 mm. Different lines correspond to various powers of heating radiation (14 W of total power corresponds to maximal intensity used in experiments). It can be seen that during the measurement time, the temperature does not exceed 220 °C. At such relatively low temperatures, compared with the softening point −1600 °C and strain point −980 °C, there are no irreversible processes occurring in the sample. Therefore, the limitations related to overheating of the fused-silica plate are inessential in our case. Nevertheless, at heating up to 220 °C there is a noticeable dependence of coefficient β and thermal conductivity coefficient on temperature, which should have an influence on the linearity of the method at high intensities.

It should be noted that the fused silica was not damaged at any intensities of heating radiation. This is due to the combination of low thermal expansion coefficient and high thermal conductivity, and to their temperature dependences. This fact was theoretically and experimentally studied in [15].

### B. Measurement Factors

We will discuss two factors that reduce the accuracy of interferometric measurements of optical thickness: spatial blurring of the interferometric pattern due to imperfect optics and temporal blurring due to relatively high time of camera exposure.

To estimate the influence of spatial blurring, which makes the interference picture observed by the CCD camera less clear, we will use the following arguments. Let us consider an interference pattern generated by the interference of two linearly polarized flat monochrome waves with intensities $I_1$ and $I_2$ incident on some surface. The wavelengths are similar and equal to λ. The first wave falls normally, the second falls at a small angle θ. The intensity distribution on the surface will be given by the formula

$$I = I_1 + I_2 + 2\sqrt{I_1 I_2}\,\cos\left(\frac{2\pi}{\lambda}x\theta\right), \tag{3}$$

if the $x$ axis is chosen in the plane of incidence. In this case, the modulation depth equals the ratio of the constant and the variable part $\Gamma = 2\sqrt{I_1 I_2}/(I_1 + I_2)$. If the pattern is observed through imperfect optics, and the spatial scale of corresponding blurring is $-d$, then one will be able to characterize the blurred intensity distribution $I_s$ through the initial one as

$$\begin{aligned} I_s(x) &= \frac{1}{d}\int_{-d/2}^{d/2} I(x)\mathrm{d}x \\ &= I_1 + I_2 + 2\sqrt{I_1 I_2}\,\frac{1}{d}\int_{-d/2}^{d/2}\cos\left(\frac{2\pi}{\lambda}x\theta\right)\mathrm{d}x, \end{aligned} \tag{4}$$

where it is possible to write down the ratio of modulation depths with blurring and without it:

$$\frac{\Gamma_s}{\Gamma} = \frac{1}{d}\int_{-d/2}^{d/2}\cos\left(\frac{2\pi}{\lambda}x\theta\right)\mathrm{d}x. \tag{5}$$

It follows from Eq. (5) that to keep $\Gamma_s$ beyond the 0.95 level with respect to the initial state, expression $d \le 0.08\lambda/\theta$ should be obeyed. The maximal angle $\theta_{max}$ can be estimated as $\theta_{max} = \Delta L_{max}/\Delta x$, where $\Delta L_{max}$ is the maximal amplitude of optical thickness variations expected in the experiment. This estimation is obtained from the belief that the heating beam contains 100% jumps of intensity, and corresponds to jumps of optical thickness blurred to the $\Delta x$ size. Hence we obtain a simple formula for maximally allowable width of blurring due to optics $d_{opt}$:

$$d_{opt} \le \frac{0.08\lambda}{2\Delta L_{max}}\,\Delta x. \tag{6}$$

Equation (6) indicates that if we set a task to observe variations with an amplitude not exceeding λ (which corresponds to the intensity of 250 W/cm$^2$ and three crossings between monotonic regions of the interference pattern) and at the same time not to worsen the spatial resolution relative to the blurring-dictated $\Delta x \sim 1$ mm resolution, then resolution of optics should be no worse than 40 μm on the fused-silica plate. It is clear that the CCD camera we use should also provide the same resolution. It is also clear that beams with a smooth intensity profile can be measured for higher maximum intensity as well.

Now we estimate temporal blurring associated with exposure time. Considerations analogous to those presented above lead to an expression for maximum exposure time $t_{\text{exp}}$:

$$t_{\text{exp}} \leq \frac{0.08\lambda}{2\Delta L_{\max}} t_m. \tag{7}$$

Equation (7) suggests that when measuring variations of the order of a wavelength, $t_m = 80$ ms after heating activation (which corresponds to two frames in the one frame method) the exposure time should not exceed 3.2 ms.

Based on these estimations, we may assert that for beam measurements with up to 250 W/cm$^2$ beam intensity at 1 mm spatial resolution, one needs to use a CCD camera with an exposure time of no more than 3.2 ms and optics with a spatial resolution of 40 μm. In this case, the measurement error will not exceed 5%. In our study, we used a CCD camera with 20 ms exposure time and 250 μm spatial resolution.

## 5. Discussion of the Results

As mentioned earlier, the experimental results demonstrate the viability of the proposed method. However, the achieved dynamical range of 0.3–3.8 W and spatial resolution of 1 mm are not very high, if we see our optical setup as a measurement device. Let us formulate what should be done to improve the suggested method.

First, higher-quality aberration-free optics should be used to enhance the dynamical range. Second, a camera with a higher frame rate or a system with holographic beam separation [16] will allow the use of a phase-modulated scheme, thus removing the limitations related to violation of monotonic dependence and improving the accuracy of measurements of optical thickness. This will result in dynamic range enhancement both toward lower and higher intensities. Third, it may be reasonable to seek a more appropriate plate material with lower thermal conductivity to improve spatial resolution of the method.

## 6. Conclusion

The experimental and theoretical investigation has confirmed the appropriateness and good prospects of the new method for intensity profile measurements. This bolometric detector is based on measurements of thermally induced variations of optical thickness of a fused-silica target. At the present stage of investigation, its sensitivity is inferior to that of classical microbolometric and, even more so, photon IR detector arrays. However, our detector may be of interest for specific applications, for instance, in profile measurements of intense IR beams of industrial $CO_2$ lasers. An essential advantage of our method is that it does not require optics and FPA for IR range, which constitute the most expensive part of existing detectors. It is worth noting that a large aperture of 60 mm has been experimentally realized and can be even further increased via improving the part of the scheme that operates in the visible light. Also important is that the suggested method may be used for profile measurements of microwave beams.

## References


1. Glenn F. Knoll, *Radiation Detection and Measurement* (Wiley, 2000).
2. V. V. Tarasov and J. G. Jakvshenko, *Infrared Systems of "Looking" Type* (Logos, 2004).
3. E. D. Pankov, A. L. Andreev, and G. V. Pol'shhikov, *Sources and Receivers of Irradiation* (Politekhnika, 1991).
4. R. W. Bogue, "US company launches first MEMS-based IR detector array," Sens. Rev. **23,** 299–301 (2003).
5. A. G. Zhukov and V. A. Mazeev, "Scanning IR-detector of bolometric array," Prikladnaja fizika, **1,** 113 (2006).
6. J. M. Fleischer and J. M. Darchuk, "Standardizing the measurement of spatial characteristics of optical beams," Proc. SPIE **888,** 60–64 (1988).
7. I. E. Kozhevatov, E. A. Rudenchik, N. P. Cheragin, and E. H. Kulikova, "Absolute testing of the profiles of large-size flat optical surfaces," Radiophys. Quantum Electron. **44,** 575–581 (2001).
8. D. Grischkowsky, S. Keiding, M. van Exter, and C. Fattinger, "Far-infrared time-domain spectroscopy with terahertz beams of dielectrics and semiconductors," J. Opt. Soc. Am. B **7,** 2006–2015 (1990).
9. V. V. Zelenogorsky, A. A. Solovyov, I. E. Kozhevatov, E. E. Kamenetsky, E. A. Rudenchik, O. V. Palashov, D. E. Silin, and E. A. Khazanov, "High-precision methods and devices for in situ measurements of thermally induced aberrations in optical elements," Appl. Opt. **45,** 4092–4101 (2006).
10. L. D. Landau and E. M. Lifshic, *Theoretical Physics. Fluid Mechanics* (Nauka, 1988).
11. A. A. Soloviev, I. E. Kozhevatov, O. V. Palashov, and E. A. Khazanov, "Compensation for thermally induced aberrations in optical elements by means of additional heating by $CO_2$ laser radiation," Quantum Electron. **36,** 939–945 (2006).
12. L. D. Landau and E. M. Lifshic, *Theoretical Physics. Theory of Elasticity* (Nauka, 1988).
13. A. V. Mezenov, L. N. Soms, and A. I. Stepanov, *Thermooptics of Solid-State Lasers* (Mashinostroenie, 1986).
14. S. Chenais, F. Balembois, F. Druon, G. Lucias-Leclin, and P. Georges, "Thermal lensing in diode-pumped ytterbium lasers—Part I: theoretical analysis and wavefront measurements," IEEE J. Quantum Electron. **40,** 1217 (2004).
15. C. Wei, H. He, Z. Deng, J. Shao, and Z. Fan, "Study of thermal behaviors in $CO_2$ laser irradiated glass," Opt. Eng. **44,** 044202 (2005).
16. http://www.4dtechnology.com/4D%20Technology.htm.